On the Robustness of an Analog VLSI Implementation of a Time Encoding Machine

Peter R. Kinget and Aurel A. Lazar
Department of Electrical Engineering,
Columbia University,
New York, NY 10027, USA

László T. Tóth
Dept. of Telecom. and Media Informatics
Budapest Univ. of Technology and Economics
Budapest, Hungary H-1117

Abstract— Time encoding is a mechanism for representing the information contained in a continuous time, bandlimited, analog signal as the zero-crossings of a binary signal. Time decoding algorithms have been developed that make a perfect recovery of time encoded bandlimited signals possible. We consider a simple one-opamp active RC implementation of the time encoder and investigate the robustness in performance of the time decoder when the former is subject to non-idealities of the analog VLSI realization. We show that up to a constant scaling factor, delay and offset the input signal can be accurately reconstructed even if the opamp has a finite DC gain and finite bandwidth and the circuit exhibits parameter offsets. We develop an experimental upper bound for the reconstruction error that can be used in the design of the encoder. The analytical results are verified with numerical simulations.

I. INTRODUCTION

The classical sampling theorem calls for reconstructing an analog signal $x(t)$ bandlimited to $[-\Omega, \Omega]$ using its amplitude samples taken uniformly at or above the Nyquist rate Ω/π. If amplitude samples $x(t_k)$ are available at irregularly spaced times t_k, the same bandlimited signal $x(t)$ can be reconstructed if the average of the durations

$$T_k = t_{k+1} - t_k \qquad (1)$$

are at or below π/Ω [1]. For signal reconstruction in the irregular sampling case, both the amplitude and time samples are required. In
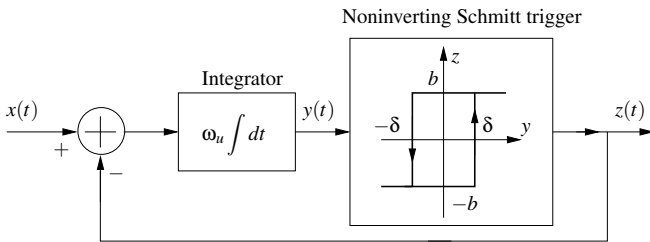
Fig. 1. The ideal time encoder.

the case of time encoding a signal-dependent sampling is carried out by a Time Encoding Machine (TEM) such that $x(t)$ can be reconstructed based on the t_k's only. The TEM investigated in [2] is shown in Figure 1. It consists of an adder, an integrator with unity-gain frequency ω_u and a noninverting Schmitt trigger with a symmetrically centered hysteresis of width 2δ and height $2b$. In what follows we assume that for some given c

$$|x(t)| \leq c < b \qquad (2)$$

holds. To simplify the notation we will also use

$$\alpha = \frac{c}{b} \quad \text{and} \quad T_0 = \frac{4\delta}{\omega_u b} \qquad (3)$$

as the bound for the normalized input $x(t)/b$ and the self-oscillation period of $z(t)$ for $x(t) = 0$, respectively.

Since the integrator's input is $x(t) \pm b$ where $|x(t)| < b$ (see (2)), its output $y(t)$ is a strictly monotonic increasing or decreasing function for $t \in (t_k, t_{k+1})$ where $z(t)$ changes sign and $y(t)$ reaches δ or $-\delta$ at $t = t_k$. A straightforward analysis [2] gives:

$$q_k = \int_{t_k}^{t_{k+1}} x(t)dt = (-1)^k b \left(\frac{T_0}{2} - T_k \right) \qquad (4)$$

It can also be shown [2] that T_k introduced in (1) is bounded as:

$$\frac{T_0}{2} \frac{1}{1+\alpha} \leq T_k \leq \frac{T_0}{2} \frac{1}{1-\alpha} \qquad (5)$$

Original Reconstruction [2]: With $g(t) = \sin(\Omega t)/(\pi t)$ as the impulse response of an ideal low pass filter of bandwidth Ω, the reconstructed signal, $x_r(t)$, is given by

$$x_r(t) = \sum_{\ell=-\infty}^{\infty} c_\ell g \left(t - t_\ell - \frac{T_\ell}{2} \right), \qquad (6)$$

where the coefficients c_ℓ are to be found. Integrating both sides of (6) from $t = t_k$ to $t = t_{k+1}$ gives $\mathbf{Gc} = \mathbf{q}$, where the vectors $\mathbf{c}$ and $\mathbf{q}$ contain the coefficients c_k, and the integrals q_k in (4), respectively, and the matrix $\mathbf{G}$ is given by

$$[\mathbf{G}]_{k,\ell} = \int_{t_k}^{t_{k+1}} g \left(t - t_\ell - \frac{T_\ell}{2} \right) dt. \qquad (7)$$

One way of solving the typically ill-conditioned linear equations $\mathbf{Gc} = \mathbf{q}$ is given by

$$\mathbf{c} = \mathbf{G}^+ \mathbf{q}, \qquad (8)$$

where $\mathbf{G}^+$ denotes the pseudo (Moore-Penrose) inverse of $\mathbf{G}$. As in the case of irregular sampling, perfect reconstruction is possible if the average density of the t_k's is below or at the Nyquist rate [2]. Based on (5) this condition is certainly satisfied if $(T_0/2)/(1-\alpha) < \pi/\Omega$.

Compensation Principle [2]: The reconstruction based on (4) relies on the accurate value of T_0. An alternative technique is based on the simple observation that due to the additive property of integrals $q_k + q_{k+1} = (-1)^k b(T_{k+1} - T_k)$ does not dependent on T_0. Forming a vector with elements $q_k + q_{k+1}$ is possible as

$$[\mathbf{Bq}]_k = \int_{t_k}^{t_{k+2}} x(t)dt = (-1)^k b(T_{k+1} - T_k), \qquad (9)$$

where matrix $\mathbf{B}$ is defined as $[\mathbf{B}]_{k,\ell} = 1$ for $k = \ell$ and $k = \ell + 1$ and $[\mathbf{B}]_{k,\ell} = 0$ otherwise. Using $\mathbf{B}$ and $\mathbf{Gc} = \mathbf{q}$ gives $\mathbf{BGc} = \mathbf{Bq}$, therefore:

$$\mathbf{c} = (\mathbf{BG})^+ \mathbf{Bq}. \qquad (10)$$

Remark 1: Perfect reconstruction can be achieved only if the dimensionality of the matrices and vectors used ($\mathbf{G}$, $\mathbf{B}$, $\mathbf{q}$, and $\mathbf{c}$) is infinite. Since in reality only a finite number of t_k's is available within some observation window $t_k \in (T_{\min}, T_{\max})$, $x_r(t)$ of (6) merely approximates $x(t)$. Due to *boundary effects* [2] the error in signal

recovery is generally larger for times closer to either boundary of the observation window, $T_{\min}$ and $T_{\max}$.

II. ACTIVE-RC TEM

Figure 2 shows an active RC implementation[1] of the encoder, where $x(t)$, $v(t)$, $y(t)$, and $z(t)$ denote node voltages. The parameters
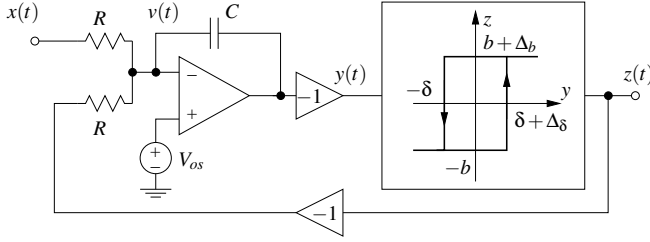
Fig. 2. An active RC implementation of the encoder in Figure 1.

Δ_δ and Δ_b model the implementation errors in the hysteresis levels $\pm\delta$ and $\pm b$, respectively. The opamp shown has infinite input and zero output impedance and an input referred offset voltage V_{os}. For $\Delta_\delta = \Delta_b = V_{os} = 0$ the circuit in Fig. 2 implements the ideal TEM of Fig. 1 with $\omega_u = 1/(RC)$.

For the input voltage $v_d(t) = V_{os} - v(t)$ the linear imperfections[2] of the opamp are modeled by the transfer function

$$A(s) = \frac{-Y(s)}{V_d(s)} = \frac{A_{DC}}{1 + s\frac{A_{DC}}{\omega_t}}, \qquad (11)$$

where A_{DC} and ω_t are the finite DC gain and unity-gain frequency (gain-bandwidth product) [3].

A. Effects of parameter errors and opamp offset

Assuming $A_{DC} \to \infty$ and $\omega_t \to \infty$, we have (see Appendix)

$$\gamma \int_{t_k}^{t_{k+2}} (x(t) - X_{os})\, dt = b(-1)^k (T_{k+1} - T_k), \qquad (12)$$

where $\gamma = b/(b + \Delta_b/2)$ and $X_{os} = 2V_{os} + \Delta_b/2$.

Comparing (12) with (9) we conclude that the reconstructed signal using the Compensation Principle is $x(t)$ except for a constant scaling factor γ and DC offset X_{os} due to opamp offset, V_{os}, and the hysteresis output level variation Δ_b. The variation in δ, Δ_δ, does not affect the encoding as long as the Compensation Principle is used for reconstruction.

B. Effects of the opamp's finite DC gain and gain-bandwidth product

To simplify the notations we assume that $\Delta_\delta = \Delta_b = 0$, and $V_{os} = 0$. The opamp's finite DC gain results in a maximum DC gain for the integrator and the creation of a (parasitic) low frequency pole ω_1; the finite gain-bandwidth product results in a (parasitic) high frequency pole, ω_2, and using (11) the transfer function for the integrator becomes [4]

$$H(s) = \frac{Y(s)}{X(s)} = \frac{Y(s)}{-Z(s)} = \frac{\omega_u \omega_2}{(s + \omega_1)(s + \omega_2)} \qquad (13)$$

[1]To simplify the diagrams and notation we show a single ended implementation whereas in an actual VLSI realization a differential implementation would be used. The realization of the -1 multipliers then corresponds to a simple crossing of wires. The presented analysis is valid for differential implementations and can also be easily adapted for alternative TEM realizations using, e.g., transconductor-C integrators.

[2]Referring to the waveforms in Fig. 3 (a) it is clear that opamp can be designed with a sufficient slew rate and output range so that no significant non-linear errors occur.

For large enough A_{DC} and ω_t, the approximations [3]

$$\omega_u \simeq \frac{1}{RC}, \quad \omega_1 \simeq \frac{2\omega_u}{A_{DC}} \quad \text{and} \quad \omega_2 \simeq \omega_t,$$

can be used. For $A_{DC} \to \infty$ and $\omega_t \to \infty$, $H(s)$ indeed becomes the ideal integrator transfer function ω_u/s.

C. Simulation example using the model in (13)

A simulation model for the active RC TEM was developed with the opamp replaced by an equivalent circuit[4] to model its finite DC gain and gain-bandwidth product and the following TEM parameters: $1/(RC) = 12$ Mrad/sec, $b = 1$ V, $\delta = 0.5$ V. A two-tone sinusoid, $x(t) = A_1 \sin(2\pi f_1 t) + A_2 \sin(2\pi f_2 t)$, where $A_1 = A_2 = 0.25$ V, $f_1 = 1$ MHz, and $f_1 = 1.5$ MHz was used as the input signal (see Figure 4(a)) so that $\Omega = 2\pi \times 1.5$ Mrad/sec and $\alpha = 1/2$. These parameters are kept fixed for all examples in this paper.

Ideal opamp: Simulations were carried out to determine $y(t)$ and $z(t)$ and 50 zero-crossings of $z(t)$ were calculated with high accuracy. The reconstructed signal, $x_r(t)$, was calculated using the original and the Compensation Principle based reconstruction. The root-mean-square (RMS) value of the reconstruction error $e(t) = x_r(t) - x(t)$ is denoted by $\mathcal{E}$. To avoid boundary effects (see Remark 1) $\mathcal{E}$ is calculated over the reduced range $t \in (t_3, t_{45})$. The reconstruction error $e(t)$ for a TEM with an almost ideal opamp, $A_{DC} = 10^7, \omega_t/\omega_u = 3 \times 10^7$, was calculated first. The original reconstruction and Compensation Principle give almost identical errors with $\mathcal{E} \le -124$ dB. This error is mostly due to the fact that only 50 t_k's were used [2].
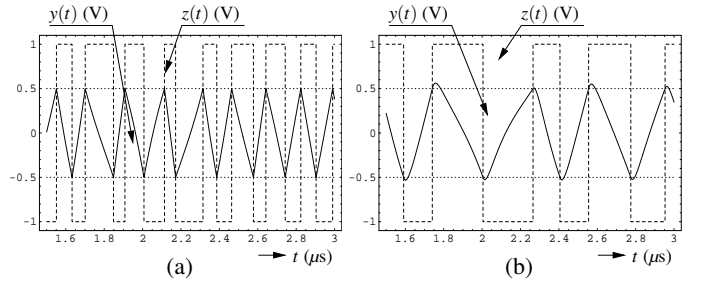
Fig. 3. Simulation results for $y(t)$ and $z(t)$ obtained by settings $A_{DC} = 10^7, \omega_t/\omega_u = 3 \times 10^7$ (a) and $A_{DC} = 10, \omega_t/\omega_u = 3$ (b).

Non-ideal opamp: Figure 3 shows $y(t)$ and $z(t)$ with nearly ideal and very non-ideal settings for the opamp. In the nearly ideal case $z(t)$ has transitions (zero-crossings) at $t = t_k$, when $y(t)$ reaches δ or $-\delta$. For the non-ideal case $y(t)$ goes noticeably above δ and below $-\delta$ at $t = t_k$ and the overall operation of the encoder is slower compared to using an (almost) ideal integrator. For the TEM with a non-ideal opamp, the signal was again reconstructed using the original and Compensation Principle. The RMS reconstruction errors, $\mathcal{E}$, are shown in Figure 4(b) for different opamp parameters: $A_{DC} = 10, 10^2, \ldots, 10^5$ and $\omega_t/\omega_u = 3, 30, 300, 3000$. Using the Compensation Principle $\mathcal{E}$ significantly improves compared to the original reconstruction.

III. ANALYSIS OF THE ERRORS DUE TO THE MODEL IN (13)

The effects of finite opamp gain and gain-bandwidth product can be analyzed using Figure 5 which is obtained by simple rearrangement

[3]In the simulation examples below the exact values for ω_1 and ω_2 were used. In the remainder of the text we also use the notation ω_t/ω_u to compare the opamp's ω_t to the integrator's ω_u. In the simulations, $\omega_t RC$ was set to the values mentioned but the error in this approximation is very small.

[4]We used a voltage controlled current source loaded with a resistor and capacitor in parallel and followed by an inverting unity-gain buffer.
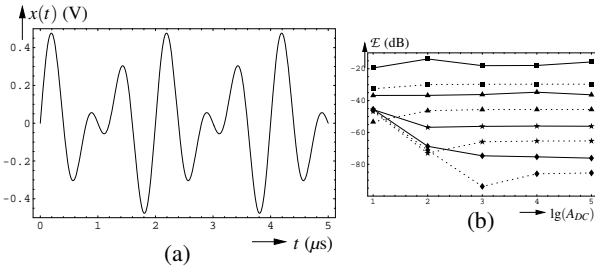
Fig. 4. (a) Input signal used in the simulations. (b) Recovery RMS error $\mathcal{E}$ in terms of $\lg(A_{DC})$ for the original reconstruction (–) and the Compensation Principle (- -) for $\omega_t/\omega_u = 3$ (■), 30 (▲), 300 (★), 3000 (◇).

of Figure 1 after replacing the integrator by $H(s)$ in (13). Using
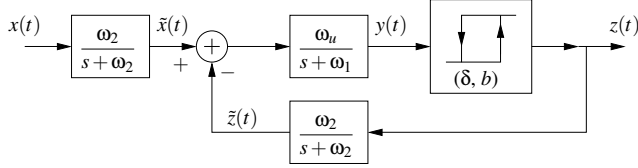
Fig. 5. The encoder in Figure 1 using the lossy integrator model in (13).

standard first-order linear circuit analysis yields (see Appendix)

$$\frac{1}{b}\int_{t_\ell}^{t_{\ell+1}} \tilde{x}(\tau)e^{-\omega_1(t_{\ell+1}-\tau)}d\tau = \frac{(-1)^\ell T_0}{4}\left(e^{-\omega_1 T_\ell}+1\right)$$
$$+\left(a_\ell+(-1)^\ell\right)\frac{e^{-\omega_1 T_\ell}-e^{-\omega_2 T_\ell}}{\omega_2-\omega_1}-(-1)^\ell\frac{1-e^{-\omega_1 T_\ell}}{\omega_1}, \quad (14)$$

where a_ℓ is given by the recursion

$$a_{\ell+1}=e^{-\omega_2 T_\ell}\left(a_\ell+(-1)^\ell\right)-(-1)^\ell. \quad (15)$$

In order to obtain approximate but simplified results we make the realistic assumptions:

$$\Omega << \omega_2, \quad \omega_1 T_\ell << 0, \quad \text{and} \quad \omega_2 T_\ell >> 0. \quad (16)$$

Slower operation of the encoder: As derived in the Appendix, the T_k's have the (approximate) bounds:

$$\left(\frac{T_0}{2}+\frac{2}{\omega_2}\right)\frac{1}{1+\alpha}\le T_\ell \le \left(\frac{T_0}{2}+\frac{2}{\omega_2}\right)\frac{1}{1-\alpha}. \quad (17)$$

A comparison of (17) with (5) shows that, in agreement with Figure 3, the operation of the encoder slowed down. Although the Schmitt trigger fires at $t=t_k$, its output $z(t)$ suffers a delay through the $\omega_2/(s+\omega_2)$ block in the feedback path. This intuitively explains why $y(t)$ in Figure 3(b) goes above δ and below $-\delta$.

Errors in the original reconstruction: For small enough ω_1 the left-hand-side (LHS) of (14) is close to q_ℓ/b in (4). For sufficiently large ω_2 (15) implies $a_\ell \simeq (-1)^\ell$ and therefore approximating the right-hand-side (RHS) of (14) for small ω_1 gives

$$q_\ell \simeq (-1)^\ell b\left(\frac{T_0}{2}+\frac{2}{\omega_2}-T_\ell\right). \quad (18)$$

By comparing this result with (4) it can be seen that the constant term $T_0/2$ is modified by $2/\omega_2$. This affects the accuracy of the original reconstruction. In agreement with the solid traces of Figure 4(b), increasing ω_2 (hence ω_t) by a factor of 10 results in about 20 dB drop in $\mathcal{E}$ provided that A_{DC} is large enough (hence ω_1 is small enough). Using the Compensation Principle based reconstruction cancels $2/\omega_2$ together with $T_0/2$ and improves $\mathcal{E}$ by approximately 10 dB. As shown next the error can be further reduced by investigating the effect of ω_2 on the input signal $x(t)$.

Input delay due to ω_2: Since $\tilde{x}(t)$, introduced in Fig. 5 is merely a slightly pre-filtered version of $x(t)$, a reconstruction for $\tilde{x}(t)$ might be acceptable in many applications. Moreover, for reasonably large ω_2 (see the Appendix)

$$\tilde{x}(t) \simeq x\left(t-\frac{1}{\omega_2}\right) \quad (19)$$

and thus $\tilde{x}(t)$ is just a delayed version of the input.

Simulation results: Here we use the same parameters and input as in Section II-C. The reconstructed signal, $x_r(t)$ is calculated using the Compensation Principle; $\tilde{\mathcal{E}}$ denotes the RMS value of the error signal $\tilde{e}(t) = \tilde{x}(t) - x_r(t)$; $\mathcal{E}_d$ is the RMS value of the error with respect to the delayed input, $e_d(t) = x(t-1/\omega_2) - x_r(t)$.

Figure 6(a) shows the simulation results for $\mathcal{E}_d$. A very substantial improvement of 20 dB or better can be seen compared to the dashed traces (Compensation Principle) of Figure 4(b). As expected from the presented analysis, an important effect of the presence of ω_2 is the creation of a delay between the input signal $x(t)$ and the encoded signal in $z(t)$. In most applications this delay is acceptable and thus the results in Figure 6(a) depict the precision that can be attained with different opamp realizations of the TEM.

Comparing $\mathcal{E}_d$ and $\tilde{\mathcal{E}}$ in Figure 6(a) we conclude that for $\omega_t/\omega_u = 3$ or 30 the approximation of the effect of ω_2 as a simple delay in (19) is not accurate. However, $z(t)$ now encodes $\tilde{x}(t)$ very accurately even for a low ω_t/ω_u of 30.

Output delays in the hysteresis: The finite output bandwidth of the hysteresis circuit results in a low pass filter in the feedback path for $z(t)$ and its model corresponds to Figure 5 but without the input $\omega_2/(s+\omega_2)$ block. Its effects can be quantified as the effects of ω_2 on the reconstruction error for $\tilde{x}(t)$. Provided that the output bandwidth of the hysteresis circuit is larger than the unity gain bandwidth of the opamp, the former will not significantly affect the TEM accuracy.

Error bound for the integrals and estimate for the RMS reconstruction error: The recovery error is intuitively expected to decrease if the reconstructed signal is compared to $\tilde{x}(t)$ of Figure 5, since the undesired prefiltering of the $\omega_2/(s+\omega_2)$ block is ignored. In particular, as shown in Appendix we have the approximation

$$\int_{t_k}^{t_{k+2}} \tilde{x}(t)dt \simeq b(-1)^k(T_{k+1}-T_k)+e_k, \quad (20)$$

where the integral error sequence e_k is bounded as:

$$|e_k| \le e_B = c\omega_1\frac{(4+\omega_2 T_0)(6-2\alpha+\omega_2 T_0)}{2(\alpha-1)^2(\alpha+1)\omega_2^2}. \quad (21)$$

Based on the integral error e_k in (20) it is not straightforward to handle the overall reconstruction error or its RMS value $\mathcal{E}_o$ analytically because of the irregular nature of the t_k's. Nevertheless, a proportionality between $\mathcal{E}$ and $\mathcal{E}_o$ certainly holds due to (10) and (6). In [2] an experimental estimate for the RMS value of the reconstruction error due to time quantization was found by approximating (modeling) i) the error as sequence of i.i.d. random variables and ii) the T_k's by their average value T_s. Following a similar line of reasoning here, $\mathcal{E}_o$ can be estimated by $\mathcal{E}\sqrt{\Omega/(\pi T_s)}$ where, based on (17), a reasonable estimate for T_s is:

$$T_s = \frac{1}{2}\left\{\left(\frac{T_0}{2}+\frac{2}{\omega_2}\right)\frac{1}{1-\alpha}+\left(\frac{T_0}{2}+\frac{2}{\omega_2}\right)\frac{1}{1+\alpha}\right\} \quad (22)$$

Therefore, using (21) a rough estimate for the RMS value of the reconstruction error bound is given by:

$$\mathcal{E}_B = \varepsilon_B\sqrt{\frac{\Omega}{\pi T_s}}. \quad (23)$$

Figure 6(b) compares the bound estimates $\mathcal{E}_B$ and the results for $\tilde{\mathcal{E}}$. For $\omega_t/\omega_u = 3$, $\mathcal{E}_B$ reaches $\tilde{\mathcal{E}}$ which is to be expected since third condition in (16) is not sufficiently satisfied ($\omega_2 \min_\ell(T_\ell) = 7.19$ for $A_{DC} = 10^5$). For larger ω_t/ω_u, $\omega_t/\omega_u > 3$, $\mathcal{E}_B$ tracks $\tilde{\mathcal{E}}$ but $\mathcal{E}_B$ is not a tight bound. This could be due to finite precision in the simulations or the approximations made in the derivation of $\mathcal{E}_B$. Most probably the main reason is the fact that after canceling a dominant common error term with the Compensation Principle, the estimation of the remaining error is hard.
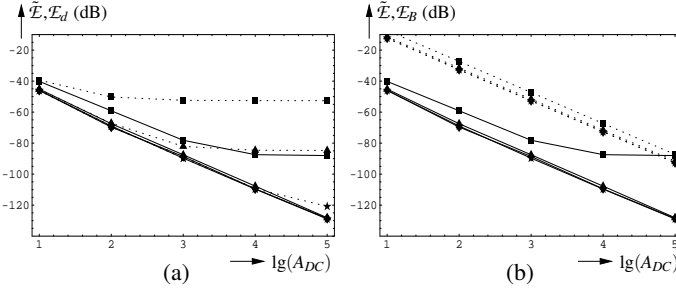
Fig. 6. Simulation results in terms of $\lg(A_{DC})$ for for $\omega_t/\omega_u = 3$ (■), 30 (▲), 300 (⋆), 3000 (◇); (a): $\tilde{\mathcal{E}}$ (–) and $\mathcal{E}_d$ (– –). (b): $\tilde{\mathcal{E}}$ (–) and $\mathcal{E}_B$ (– –).

IV. DISCUSSION

The analysis and simulation results presented in this paper show that the TEM operation is robust with respect to VLSI implementation non-idealities. Offsets and some variations in the building block parameters only lead to offsets and scaling factor in the encoded signal. Other parameter variations are completely canceled. The requirements on the integrator circuit can be derived from Figure 6(a). For example, with an opamp DC gain of 60 dB and gain-bandwidth product ω_t of 30 times the integrator unity gain frequency ω_u, the RMS errors remains below -80 dB. For a DC gain of 80 dB and $\omega_u = 300\omega_t$ the errors are below -110 dB. Such opamp requirements are similar to, *e.g.*, the requirements for opamps for continuous time filters [4] or analog to digital converters [3]. Due to space limitations, we could not address here the robustness properties of the time decoder with respect to thermal noise disturbances arising in the time encoder. These and related questions will be addressed elsewhere.

APPENDIX

Proof of (12): For an ideal opamp $v(t) = V_{os}$, and thus the encoder in Figure 2 is described by the circuit equation $(x - V_{os})/R + (-z - V_{os})/R + Cd(-y - V_{os})/dt = (x - V_{os})/R - (z + V_{os})/R - Cdy/dt = 0$. By integrating both sides above from t_ℓ to $t_{\ell+1}$ we obtain:

$$y(t_{\ell+1}) - y(t_\ell) = \int_{t_\ell}^{t_{\ell+1}} \frac{x(t) - V_{os}}{RC} dt - \int_{t_\ell}^{t_{\ell+1}} \frac{z(t) + V_{os}}{RC} dt$$

Adding this relationship for $\ell = k$ and $\ell = k+1$ and noting that (without loss of generality) $y(t_\ell) = -(-1)^\ell \delta + (1 - (-1)^\ell)\Delta_\delta/2$ and $z(t) = -(-1)^\ell b + (1 - (-1)^\ell)\Delta_b/2$ for $t \in (t_\ell, t_{\ell+1})$ gives (12).

Proof of (14) and (15) : In terms of the $\omega_u/(s + \omega_1)$ block and the $\omega_2/(s + \omega_2)$ block in the feedback path of Figure 5 we have

$$y(t) = e^{-\omega_1(t-t_\ell)} y(t_\ell) + \omega_u \int_{t_\ell}^t (\tilde{x}(\tau) - \tilde{z}(\tau)) e^{-\omega_1(t-\tau)} d\tau \quad (24)$$

and

$$\tilde{z}(t) = e^{-\omega_2(t-t_\ell)} \tilde{z}(t_\ell) + \omega_2 \int_{t_\ell}^t z(\tau) e^{-\omega_2(t-\tau)} d\tau, \quad (25)$$

respectively, for some $t \in (t_\ell, t_{\ell+1}]$. Due to the presence of the Schmitt trigger, $y(t_\ell) = -(-1)^\ell \delta$ and $z(t_\ell) = -(-1)^\ell b$. Using these

relationships with $a_\ell = \tilde{z}(t_\ell)/b$ and T_0 defined in (3) in evaluating (24) and (25) at $t = t_{\ell+1}$ gives (14) and (15).

Proof of (17): Expressing $\tilde{x}(t)$ as a convolution and using (2) gives:

$$\tilde{x}(t) = \int_0^\infty x(t-\tau)\omega_2 e^{-\omega_2\tau} d\tau \leq c \int_0^\infty \omega_2 e^{-\omega_2\tau} d\tau = c. \quad (26)$$

Using the third condition of (16) in (15) gives $a_{\ell+1} \simeq -(-1)^\ell$. Therefore the RHS of (14) can be approximated by $(-1)^\ell(T_0/2 + 2/\omega_2 - T_\ell)$. By applying the mean value theorem the integral on the LHS of (14) can be expressed as $T_\ell \tilde{x}(\xi_\ell) e^{-\omega_1(t_{\ell+1} - \xi_\ell)} \simeq T_\ell \tilde{x}(\xi_\ell) \leq T_\ell c$ with appropriate $\xi_\ell \in [t_\ell, t_{\ell+1}]$. Combining these relationships gives the inequality $(-1)^\ell T_\ell c/b \geq T_0/2 - 2/\omega_2 - T_\ell$ that can be solved for T_ℓ (depending on ℓ being even or odd) and (17) follows.

Proof of (19): Let $X(\omega)$ be the Fourier transform of $x(t)$. Then, using the transfer function $\omega_2/(j\omega + \omega_2) = \omega_2 e^{-j\arctan\omega/\omega_2}/\sqrt{\omega^2 + \omega_2^2}$ corresponding to the $\omega_2/(s + \omega_2)$ block in Fig. 5 and the inverse Fourier transform representation gives:

$$\tilde{x}(t) = \frac{1}{2\pi} \int_{-\Omega}^{\Omega} X(\omega) \frac{\omega_2}{\sqrt{\omega^2 + \omega_2^2}} e^{j\omega t - j\arctan\left(\frac{\omega}{\omega_2}\right)} d\omega.$$

With the first assumption in (16) and noting that the integration range is carried out over $\omega \in (-\Omega, \Omega)$ we obtain $\omega_2/\sqrt{\omega^2 + \omega_2^2} \simeq 1$ and $\arctan(\omega/\omega_2) \simeq \omega/\omega_2$. Therefore

$$\tilde{x}(t) \simeq \frac{1}{2\pi} \int_{-\Omega}^{\Omega} X(\omega) e^{j\omega\left(t - \frac{1}{\omega_2}\right)} d\omega = x\left(t - \frac{1}{\omega_2}\right)$$

in agreement with (19).

Proof of (20) and (21): Rearranging (14) and approximating by using (16) and (26) gives:

$$\int_{t_\ell}^{t_{\ell+1}} \tilde{x}(\tau) \simeq \overbrace{\int_{t_\ell}^{t_{\ell+1}} \tilde{x}(\tau)\left(1 - e^{-\omega_1(t_{\ell+1} - \tau)}\right)}^{\leq c\int_{t_\ell}^{t_{\ell+1}}\left(1 - e^{-\omega_1(t_{\ell+1} - \tau)}\right) \simeq \frac{c}{2}\omega_1 T_k^2}$$
$$+ 2b(-1)^\ell \frac{1 - \omega_1 T_\ell}{\omega_2} + b\frac{(-1)^\ell T_0}{4}(-\omega_1 T_\ell + 2).$$

Adding this relationship for $\ell = k$ and $\ell = k+1$ gives (20) with

$$e_k \leq \frac{c}{2}\omega_1(T_k^2 + T_{k+1}^2) + (-1)^k \omega_1 (T_{k+1} - T_k)\left(\frac{2}{\omega_2} + \frac{T_0}{4}\right).$$

¿From (17) we obtain $T_k^2 + T_{k+1}^2 \leq 2(T_0/2 + 2/\omega_2)^2/(1 - \alpha^2)$ and $|T_{k+1} - T_k| \leq (T_0/2 + 2/\omega_2)(1/(1 - \alpha) - 1/(1 + \alpha))$ and the bound in (21) follows.

REFERENCES

[1] S. Jaffard, S., "A Density Criterion for Frames of Complex Exponentials," *Michigan Mathematical Journal*, vol. 38, no. 3, pp. 339-348, 1991.
[2] A. A. Lazar and L. T. Tóth, "Perfect recovery and sensitivity analysis of time encoded bandlimited signals," *IEEE Transactions on Circuits and Systems-I: Regular Papers*, vol. 51, no. 10, pp. 2060-2073, October 2004.
[3] P. R. Gray, P. J. Hurst, S. H. Lewis, and R. G. Meyer, *Analysis and Design of analog integrated circuits*, 4th ed. New York, NY (USA): John Wiley & Sons, 2001.
[4] Y. Tsividis and J. Voorman, *Integrated Continuous-time filters*. New York: IEEE Press, 1993.